

Repository Istituzionale dei Prodotti della Ricerca del Politecnico di Bari

Spider Silks Mechanics: Predicting Humidity and Temperature Effects

This is a pre-print of the following article

Original Citation:
Spider Silks Mechanics: Predicting Humidity and Temperature Effects / Fazio, V., De Tommasi, D., Maria Pugno, N., Puglisi, G.. - In: JOURNAL OF THE MECHANICS AND PHYSICS OF SOLIDS. - ISSN 0022-5096. - STAMPA. - 164:(2022). [10.1016/j.jmps.2022.104857]

Availability:
This version is available at http://hdl.handle.net/11589/236965 since: 2022-03-27

Published version
DOI:10.1016/j.jmps.2022.104857

Publisher:

Terms of use:

(Article begins on next page)

16 November 2026

Spider Silks Mechanics: Predicting Humidity and Temperature Effects

Vincenzo Fazio[1], Domenico De Tommasi[2], Nicola Maria Pugno[3*], Giuseppe Puglisi[2**].

[1] *Laboratory of Bio-Inspired and Graphene Nanomechanics, University of Trento, Via Mesiano 77, 38123 Trento, Italy;*

[2] *Dip. Scienze Ingegneria Civile e Architettura, Politecnico di Bari, Via Re David 200, Bari, Italy*

[3] *Laboratory of Bio-Inspired and Graphene Nanomechanics, University of Trento, Via Mesiano 77, 38123 Trento, Italy;*
School of Engineering and Materials Science, Queen Mary University of London, Mile End Road, London E1 4NS, U.K.

[*] *nicola.pugno@unitn.it*

[**] *giuseppe.puglisi@poliba.it*

Abstract

We deduce a microstructure inspired model for humidity and temperature effects on the mechanical response of spider silks, modeled as a composite material with a hard crystalline and a soft amorphous region. Water molecules decrease the percentage of crosslinks in the softer region inducing a variation of natural length of the macromolecules. The resulting kinematic incompatibility between the regions crucially influences the final mechanical response. We demonstrate the predictivity of the model by quantitatively reproducing the experimentally observed behavior.

Keywords: Spider silk; Humidity; Biopolymers; Micromechanically-based models; Supercontraction

1. Introduction

Due to their extraordinary properties, spider silks represent one of the most intensively studied materials, also in the spirit of biomimetics [**?**]. The availability of more and more sophisticated experimental techniques let in the last

decades a deeper understanding –both from a chemical and structural point of view– of the complex multiscale, hierarchical material structure at the base of their notable mechanical behavior. Nevertheless, due to the complexity of its behavior, many important phenomena regulating its loading history dependence, rate, temperature and humidity effects, remain unclear [**?**], especially when multiscale effects are taken in consideration. In this paper we propose a model for describing and predicting humidity and temperature effects and with a special focus on a crucial phenomenon known as *supercontraction* effect. Firstly addressed in [**?**], it consists in a shrinkage of the fiber up to 50% of its initial length, when immersed in water or in high humidity environment strongly modifying the mechanical performances. As we show, the comprehension of such striking behavior let us deduce a predictive model for the experimental thermohygromechanical behavior of spider silks, starting from a description at the molecular scale.

At the molecular scale, spider silks are composed by an amorphous matrix of oligopeptide chains and by pseudo-crystalline regions made up principally of polyalanine β-sheets [**?** **?**] with dimensions between 1 and 10 nm [**?**], mostly oriented in the fiber direction [**?**]. The cross section of the fiber is highly organized in the radial direction [**?** **?** **?**]. Moreover, the chemical and structural composition varies according with the different silks produced by the different glands [**?**] and of course the different species. Here, to fix the ideas, we focus on the most performant case of dragline silk.

More in detail, the thread is covered by a skin, with a chemical and physical protection function, that does not play a role in supercontraction and mechanical response [**?**]. We thus neglect it in the model. Next, the core can be schematically decomposed as in Fig. 1. The major constituent of the external part [**?** **?**] are proteins (Major ampullate Spidroin 1, MaSp1) organized into β-pleated sheets. We refer to this fraction as *hard region*. The internal part, here referred as *soft region*, is instead mainly constituted by proteins with a proline content preventing the formation of β-sheet structures [**?**] (Major ampullate Spidroin 2, MaSp2). This fraction has a significantly lower crystallinity and

macromolecules with weaker crystal domains, typically in the form of α-helix and β-turns [**?** **?**]. The different crystallinity is also due to the shear stress at the spinning duct wall inducing the formation of harder crystal domains in form of β-sheets mainly in the outer region [**?** **?**].

Based on the previous description and referred literature, we model the silk fiber as a composite material with a hard external fraction of crystalline chains and a soft internal fraction of amorphous chains. Moreover, by following the classical approach for polymeric and biopolymeric materials [**?**], we suppose that the hard and soft fractions of macromolecules aligned with the fiber axis are embedded in a tridimensional elastic matrix, describing the complex macromolecular network with inner and intrachains connections.

Due to the different crystalline composition, the humidity affects differently the hard and soft fraction. Water hardly breaks the H-bonds of the compact β-sheet domains in the hard fraction [**?**]. On the other hand, here, we may observe a misalignment of the crystals with respect of the fiber direction that increases as the relative humidity RH grows [**?**]. Since the material stiffness grows with the alignment of the crystals [**?**], water induces a progressive damage in this fraction that we introduce in our model. On the contrary, water content strongly influences the crystal percentage in the soft internal core [**?** **?** **?**], because α-helices and β-turns are much more easily broken by water molecules. In particular, the experiments exhibit a non uniform variation of the silk properties with a localized transition at a specific value of RH, hereon indicated as RH_c, known as *supercontraction* threshold [**?**]. Finally, an important effect in the evolution of the natural chain length is induced from the stretch history (see [**?**] and reference therein for a theoretical detailed discussion of such phenomenon). Indeed, as the end-to-end distance of the molecules changes, β-sheets undergo unravelling with a corresponding increase of the number of available monomers, here considered in the hard fraction.

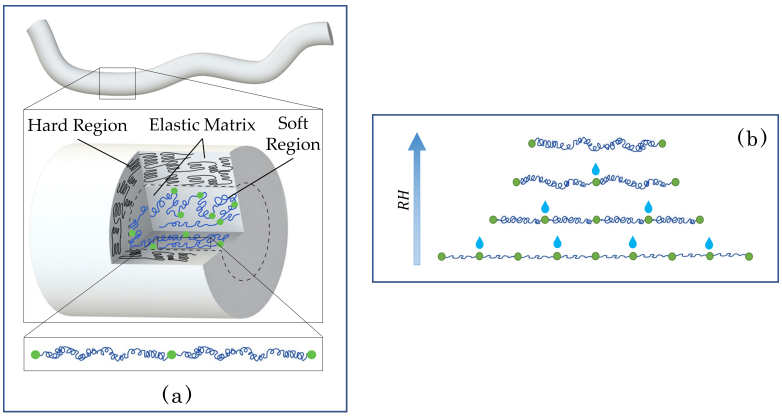


Figure 1: Cartoon of the silk fiber and its microstructure (a). The outer hard region characterized by crystals of β-sheets is represented by black chains, the soft region molecules are drafted in blue, whereas the embedding elastic matrix is grey. In (b) we schematize the incremental effects of water molecules (added as RH increases) disrupting crystal domains (green dots) and inducing entropic recoiling of chains.

2. Model

According with classical Statistical Mechanics results [**?**], the expectation value of the end-to-end distance for ideal chains is

$$L_n =< r^2 >^{1/2}= b\, n^{1/2}, \tag{1}$$

where n is the number of Kuhn segments with length b. We refer to the end-to-end distance as natural length for the reason that it is the length that the chain naturally assumes when no force is applied. As we will detail later n depends on humidity in the soft fraction, whereas it depends on the maximum attained stretch in the hard fraction. As a result the natural length of these fractions, assumed identical after spinning, vary depending on the external force and humidity fields, inducing a kinematic incompatibility as detailed in the following. We remark that in the recent paper [**?**], based on this observation, the authors proposed a model with a material undergoing a hard→soft transition reproducing a mutation from glassy to rubbery state induced by RH variations, efficiently describing the variations of stiffness and supercontraction length in correspondence of the supercontraction threshold.

2.1. Soft Region

To consider the disruption process of H-bonds induced by hydration [**?**], let us introduce the function $m = \hat{m}(\mathrm{RH})$ assigning the number of links in the generic humidity state, with $m(0) = m_o$ and $m(100) = m_f$ (initial and permanent number of H-bonds) [**?**]. To the knowledge of the authors, no direct measurement of $\hat{m}$ is available, so that we consider a Gaussian probability density of rupture events

$$d(\mathrm{RH}) = \frac{\hat{m}(\mathrm{RH}) - m_o}{m_f - m_o} = \int_0^{\mathrm{RH}} \frac{1}{\sqrt{2\pi\bar{s}^2}}\, e^{-\frac{(\mathrm{RH}-\mathrm{RH}_c)^2}{2\bar{s}^2}}. \tag{2}$$

Here $d \in (0,1)$ is a 'damage' type parameter, measuring the percentage of broken links and we assume that the Gaussian is centered in the critical value RH_c (see Fig. 2).

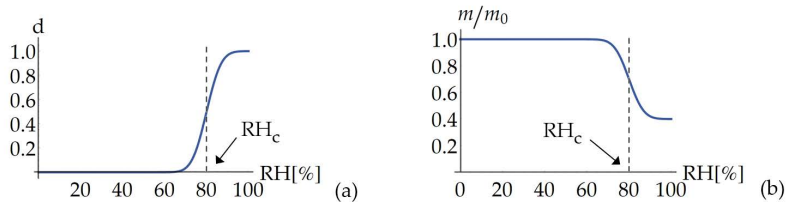


Figure 2: (a) Damage parameter d representing the percentage of broken links as a function of humidity. (b) Influence of the relative humidity on the number of H-bonds with respect to the initial number of H-bond. Here $\mathrm{RH}_c = 80\%$, $\bar{s} = 5.5$ and $m_f/m_o = 0.4$.

To obtain the corresponding variation of the natural length based on (1), assume that n_o^s is the (mean) number of chain free monomers when the silk is spun. Here and in the following we indicate by the apexes s, h, m, and t the soft, hard, matrix and homogenized (total) quantities. If we identify the number of H-bonds with the number of domains in which the chain is divided (see the scheme Fig. 1(b)), the mean number of free monomers in each domain is $n^s = \hat{n}^s(\mathrm{RH}) = n_o^s/\hat{m}(\mathrm{RH})$ corresponding to a *natural length*

$$L_n^s = \hat{m}(\mathrm{RH})\sqrt{n_o^s/\hat{m}(\mathrm{RH})}\, b^s = \sqrt{n_o^s\, \hat{m}(\mathrm{RH})}\, b^s. \tag{3}$$

We obtain in this way an analytic measure of the shrinkage chain effect induced by humidity. Observe that instead the *contour length* is fixed: $L_c^s = n^s\, b^s$.

2.2. Hard Region

As anticipated, following [**?**] we assume that the elastic modulus of the crystalline region decreases with RH by considering a (phenomenological) damage function in the macroscopic model deduced in section 2.3. On the other hand, while β-sheet crystals are affected only in their orientation by humidity, large strain can induce important unravelling effects as fully described in [**?**] with conformational transitions inside the secondary structure [**?** **?**], from a coiled configuration [**?**] to an unfolded state [**?** **?**] (see the scheme in Fig. 3). Thus the mean number n^h of available free monomers depends on the maximum attained value of the end-to-end distance so that we assume the existence of a function $\hat{n}$ such that $n^h = \hat{n}^h(L^h_{max})$. Observe that for simplicity we assume that the unfolding is irreversible with n^h monotonically increasing with L_{max}. More general hypotheses could be introduced [**?**] and a discussion of this function will be given later.

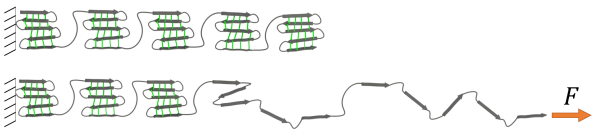


Figure 3: Cartoon of a chain of the hard region undergoing a folded → unfolded transition when subjected to a force.

As a result for the hard fraction the natural and contour lengths are assigned as

$$L^h_n = \sqrt{\hat{n}^h(L_{max})}\, b^h, \qquad L^h_c = \hat{n}^h(L_{max})\, b^h. \tag{4}$$

2.3. From single chain to macro laws

Both in the amorphous and crystalline region we adopt a Worm Like Chain (WLC) energy density (per unit chain contour length L_c) in the form proposed in [**?**] $\varphi_e = \varphi_e(L, L_c) = \kappa \frac{L^2}{L_c - L}$ where $\kappa = \frac{k_B T}{4 l_p}$, T is the temperature, k_B the Boltzmann constant and l_p the persistence length measuring the flexibility of the chain (see *e.g.* [**?**] for details). This energy respects the limit extensibility condition, $\lim_{L \to L_c} \varphi_e(L, L_c) = +\infty$, and allows for explicit calculations.

Moreover, following [**?**], we extend this function to consider that, as described above, the end-to-end distance L can be decomposed in a variable (zero force) natural length measured by (1) and the remaining length measuring the elastic elongation $L_e = L - L_n$. Thus we assume an energy and a force-elongation law for a single chain

$$\begin{aligned} \varphi_e &= \kappa \frac{L_e^2}{L_c - L} \\ f &= \frac{\partial \varphi_e}{\partial L} = \kappa \left[\left(\frac{L_c - L_n}{L_c - L} \right)^2 - 1 \right], \end{aligned} \tag{5}$$

with the force decreasing to zero as the length attains its (history dependent) natural length ($L = L_n$ or $L_e = 0$).

Notice that the total energy considering all the chains of the network can be determined as $\Phi = N_v \varphi_e L_c = N_a N_l \varphi_e L_c = N_a \varphi_e$ where for the sake of simplicity we consider $N_l L_c = 1$, with N_v, N_a, N_l the number of chains per unit volume, area, length respectively.

We remark that the proposed model can be inscribed in the theory of Thermodynamics with internal variables [**?**] in the simple case when there is a single external variable L and a single internal variable L_{max}. In our simple setting of isothermal processes, to verify the thermodynamic consistency of the model we consider the Clausius-Duhem inequality, requiring the positivity of the dissipation rate $\Gamma = f\dot{L} - \dot{\varphi}_e(L, L_{max}) \geq 0$. Since at given RH the only material fraction involved in the dissipation is the hard one, undergoing unfolding effects and variations of the natural length regulated by L_{max} according with (4), the internal energy dissipation rate reduces to $Q'(L_{max}) = -\partial_{L_{max}} \varphi_e(L, L_{max})$. Thus, in view of (5), we obtain $\Gamma = Q'(L_{max}) \dot{L}_{max} \geq 0$ that is satisfied under our assumption that $\hat{n}^h$ is increasing.

Eventually, to obtain the macroscopic behavior of the thread we consider, following [**?**], the classical *affinity hypothesis* [**?**] that identifies the macroscopic stretches with the macromolecular ones. We then first evaluate the following

stretch measures of the different fractions

$$\begin{aligned}
\lambda^i &= \tfrac{L}{L^i_o} \quad \text{total stretch,} \\
\lambda^i_e &= \tfrac{L^i_e}{L^i_o} \quad \text{elastic stretch,} \\
\lambda^i_n &= \tfrac{L^i_n}{L^i_o} \quad \text{permanent stretch,} \\
\lambda^i_c &= \tfrac{L^i_c}{L^i_o} \quad \text{contour stretch,}
\end{aligned} \qquad i = h, s, m, t, \tag{6}$$

115 with $L^i_o = b^i \sqrt{n^i_0}$ denoting the initial natural length of the chain. in particular, the permanent stretch measures the variation of the natural length, having the same role of plastic streth in classical non linear plasticity theories (see [**?**] for a detailed theoretical discussion).

For the soft region, it can be deduced using Eqns. (3) and (6),

$$\lambda^s_n = \frac{L^s_n}{L^s_o} = \frac{\sqrt{n^s_o\ \hat{m}(\mathrm{RH})}\ b^s}{\sqrt{n^s_o\ m_o}\ b^s} = \sqrt{\frac{\hat{m}(\mathrm{RH})}{m_o}}. \tag{7}$$

If we consider a Gaussian distribution for the breaking rate of the bonds as in Eqn. (2) we get the following evolution of the permanent stretch as RH varies

$$\lambda^s_n = \sqrt{1 + d(\mathrm{RH}) \left(\frac{m_f}{m_o} - 1 \right)}. \tag{8}$$

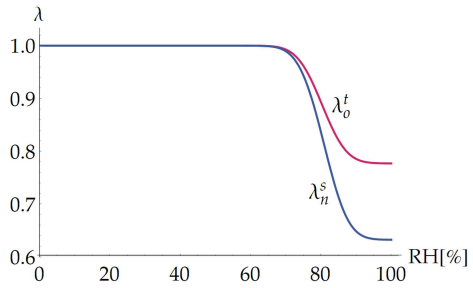


Figure 4: Dependence of the permanent stretch of the soft region λ^s_n from the relative humidity, in blue (assumed parameters $\bar{s} = 5.5$ and $m_f/m_o = 0.4$). Observe the abrupt decrease around the supercontraction threshold $\mathrm{RH}_c = 80\%$. For comparison, the unstressed stretch of the overall fiber λ^t_o is represented in pink (assumed parameters $E^s = 1.35$ MPa, $\mu = 2.5$ MPa, $\lambda^s_c = 2.62$).

A typical variation of the damage function and number of domains under our Gaussian probability choice is represented in Fig. 2, whereas the variation

of the permanent stretch of the soft fraction is reported in Fig. 4. We remark that the parameters needed to compute the variation of the permanent stretch as a function of humidity are m_f/m_o, together with RH_c and $\bar{s}$ assigning the Gaussian distribution function. On the other hand, the corresponding expression for the contour length is $L_c^s = m\frac{n_o^s}{m}\, b^s = n_o^s b^s$, so that the contour stretch of the amorphous part is constant

$$\lambda_c^s = \frac{L_c^s}{L_o^s} = \frac{n_o^s\, b^s}{\sqrt{n_o^s\, m_o}\, b^s} = \sqrt{\frac{n_o^s}{m_o}}. \tag{9}$$

Under an additive assumption and given the number of chains per unitary reference area N_a^s, the (Piola, engineering) stress using Eqns. $(5)_2$ and (6) is given by

$$\sigma^s = E^s \left[\left(\frac{\lambda_c^s - \hat{\lambda}_n^s(\mathrm{RH})}{\lambda_c^s - \lambda^s} \right)^2 - 1 \right], \tag{10}$$

where the permanent and contour stretches are given by Eqns. (8) and (9), whereas $E^s = N_a^s \kappa^s$ is the elastic modulus of the soft fraction.

For the hard region, the contour and permanent stretches are calculated by using Eqns. (4) and (6). Let n_o^h be the initial number of available free monomers, the initial natural length $L_o^h = \sqrt{n_o^h}\, b^h$ can be used to calculate the contour stretch as

$$\lambda_c^h = \frac{L_c^h}{L_o^h} = \frac{n^h b^h}{\sqrt{n_o^h}\, b^h} = \frac{n^h}{\sqrt{n_o^h}} = \frac{\hat{n}^h(\lambda_{max})}{\sqrt{n_o^h}} \tag{11}$$

and the permanent stretch as

$$\lambda_n^h = \frac{L_n^h}{L_o^h} = \frac{\sqrt{n^h}\, b^h}{\sqrt{n_o^h}\, b^h} = \sqrt{\frac{n^h}{n_o^h}} = \sqrt{\frac{\hat{n}^h(\lambda_{max})}{n_o^h}}. \tag{12}$$

Since the effective stretch-induced unfolding depends on the unknown size and strength crystals distribution, following [**?**] we assume a simple power law

$$\lambda_c^h = c_1 (\lambda_{max}^h)^{c_2}. \tag{13}$$

On the other hand, since by Eqn. (4) the permanent and contour stretches are related by $\lambda_n^h = \left(\lambda_c^h/\lambda_{co}^h\right)^{\frac{1}{2}}$, where $\lambda_{co}^h \equiv c_1$ is the initial contour stretch, by Eqn. (13) the permanent stretch is given by

$$\lambda_n^h = (\lambda_{max}^h)^{\frac{c_2}{2}}. \tag{14}$$

It is important to stress that thanks to previously described microstructure based analysis of the permanent and contour stretches, they are analytically related, so that in this fraction the permanent stretches are directly related to damage, both measured by the unknown function $\hat{n}^h$, here assumed depending on the two only parameters c_1 and c_2.

If then, as anticipated, we consider a damage taking care of the described humidity induced crystal misalignment, the stress-stretch relation for the hard part by using Eqns. (5) and (6) is

$$\sigma^h = \hat{E}^h(\mathrm{RH}) \left[\left(\frac{\hat{\lambda}_c^h(\lambda_{max}^h) - \hat{\lambda}_n^h(\lambda_{max}^h)}{\hat{\lambda}_c^h(\lambda_{max}^h) - \lambda^h} \right)^2 - 1 \right] \tag{15}$$

with

$$\hat{E}^h(\mathrm{RH}) = (1 - \alpha \ \mathrm{RH}) E_o^h, \tag{16}$$

where $E_o^h = N_a^h \kappa^h$ is the modulus in the dry condition and α measures the humidity induced damage rate.

This macroscopic constitutive damage assumption is based on the experimental observation, recalled above, of a crystal misalignment induced by humidity. Indeed, the Wide-Angle X-ray Scattering (WAXS) measurements reported in Fig. 5(a) and reproduced from [**?**], indicate a linear dependence of the Full Width at Half Maximum (the statistical measure of the orientation of crystalline β-sheets adopted in [**?**]) from RH, indicating a lower orientation of the nano crystals at higher RH values. Such misalignment affects the elastic modulus described in [**?**]. The resulting modulus variation assumed in (16) is represented in Fig. 5(b).

Eventually, by following [**?**], we consider a matrix embedding hard and soft fractions describing the complex macromolecular network composing the spider thread, with inner and intrachains connections. The total free energy is then calculated as the sum of the energy of ideally isolated hard and soft chains described above and elongated along the fiber direction plus an energy term taking care of chains interactions. Under a simple Neo-Hookean assumption (corresponding at the molecular scale to harmonic network chains [**?**]) for

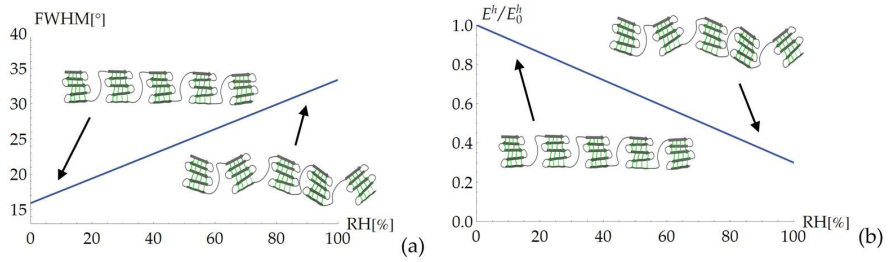


Figure 5: (a) WAXS measurements of dragline silk fibers at different RHs are used to calculate the orientation of crystalline β-sheets with respect to the fiber axis [**?**] with the result that FWHM linearly increases with RH. This proves a reduced orientation of the nano crystals under higher values of RH as schematized by the cartoons. (b) Corresponding damage function in (16): the reduction of the elastic modulus of the hard part is associated to the lack of orientation of the crystal as the humidity increases. Here we assume $\alpha = 0.007$.

incompressible material, the matrix stress for a uniaxial extension is

$$\sigma^m = \mu \left(\lambda^h - \frac{1}{(\lambda^h)^2} \right), \tag{17}$$

with μ the material shear modulus. Observe that we assume that the matrix natural length coincides with the hard fraction initial one, so that $\lambda^m = \lambda^h$.

We are now in the position of deducing, based on all the microstructure based assumptions and the affinity hypothesis, the macroscopic behavior of the spider thread. Our deduction is based on the main assumption that the spun initial length of the fractions are the same: $n^h b^h = n^s b^s$ (kinematic compatibility). After exposition to humidity the soft region chains reduce their natural length (see Fig. 6). The kinematic compatibility then imposes that the different regions undergo the same stretch λ_o^t that corresponds to zero overall initial stress. On the other hand, when the fiber is subjected to a force $F > 0$, it undergoes a stretch λ^t, starting from the new natural configuration λ_o^t. As a final result, the stretches for the soft region (that varies its permanent stretch according to humidity), hard region and matrix starting from the spun initial length (see the scheme in Fig. 7) are given by $\lambda^s = \lambda^h = \lambda^m = \lambda^t \lambda_o^t$, where λ^t represents the experimentally measured stretch.

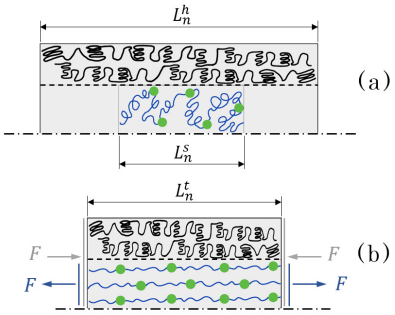


Figure 6: Outer and inner regions have different natural lengths (a) leading to a prestretch of the internal amorphous part (b).

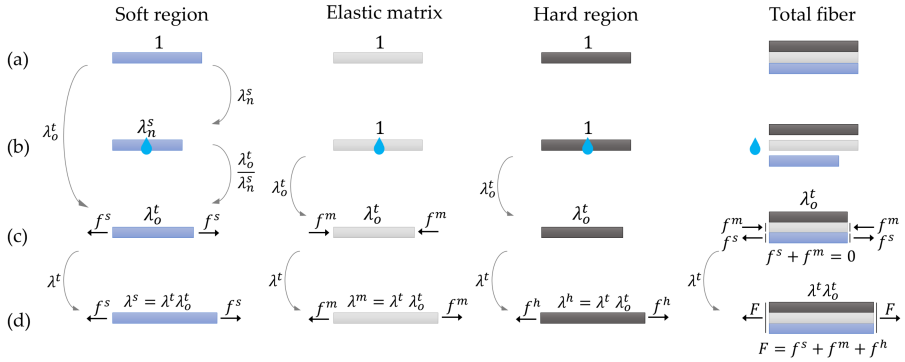


Figure 7: Scheme of the evolution of the configurations of the different composing phases and of the whole fiber: (a) dry natural configuration, (b) humid condition without external forces where selfstresses (reported in (c)) are induced by kinematic compatibility, (d) non zero external force configurations.

The overall stress-stretch relation is

$$\sigma^t(\lambda^t) = \Theta(\lambda_n^h - \lambda^t\lambda_o^t)(1-\alpha\ \mathrm{RH})E_o^h\left[\left(\frac{\lambda_c^h - \lambda_n^h}{\lambda_c^h - \lambda^t\lambda_o^t}\right)^2 - 1\right]$$

$$+E^s\left[\left(\frac{\lambda_c^s - \lambda_n^s}{\lambda_c^s - \lambda^t\lambda_o^t}\right)^2 - 1\right] + \mu\left(\lambda^t\lambda_o^t - \frac{1}{(\lambda^t\lambda_o^t)^2}\right) \tag{18}$$

where Θ is the step function considering that the hard fraction chains are not able to sustain any compressive force ($\sigma^h = 0$ if $\lambda^h < \lambda_n^h$). Observe that from this equation at $\lambda^t = 1$ and $\sigma^t = 0$ we determine λ_o^t.

155 In Fig. 8 we describe the behavior of the model here proposed, representing

the stress-stretch curves for different humidity conditions ($\mathrm{RH} = 0\%, 70\%, 85\%, 90\%, 100\%$). In the dry condition ($\mathrm{RH} = 0\%$) the natural length of the hard and soft fraction coincide ($\lambda_n^h = \lambda_n^s$) and the hard fraction participates to the mechanical response from the beginning. Consequently the force is carried mainly by the much stiffer hard fraction for all the elongation set. The behavior is similar for $\mathrm{RH} < \mathrm{RH}_c$ where a lower stiffness is due to the hard domain disorder inducing a damage according with Fig. 5 and Eqn. 12 (see the curve $\mathrm{RH} = 70\%$). Once $\mathrm{RH} > \mathrm{RH}_c$, the role played by the amorphous fraction becomes much more relevant because its natural length λ_n^s undergoes a significant decrease (see Fig. 4). This leads to a consequent substantial decrease of the initial (zero force) length of the total fiber λ_o^t. Thus, as long as the fibrils of the hard region do not reach again their natural length, the mechanical response is given only by the amorphous phase and the matrix (see *e.g.* point P_1 in Fig. 8). Then, as soon as the hard region starts to be stretched (point P_2) the force starts again to be mainly sustained by the stiffer crystalline phase (see *e.g.* point P_3). In this way we give a theoretical interpretation, in full agreement with the experiments (see Fig 9 and Fig. 9), of the 'localized' material hardening observed in spider threads . The behavior is similar also for higher values of the humidity ($\mathrm{RH} = 90\%$), with different values of λ_t distinguishing the two regimes. At extreme humidity conditions (last curve at $\mathrm{RH} = 100\%$) the mechanical behavior may be given by the only amorphous phase and matrix if the ultimate stretch of the fiber is lower than the transition threshold.

Even though in this paper we are focussed on humidity effects on monotonic stress-stretch curves, in Fig. 8 we also show through dashed lines the system behavior when subjected to unloading. This figure let us show that, based on the microstructure interpretation, the proposed model is able to describe not only the fundamental macroscopic damage effect, but also the experimentally observed presence of residual stretches [**?**]. Interestingly, permanent deformations are not deduced as usually independently from damage, *e.g.* through the introduction of new variables, whereas both damage and residual stretches descend from the unfolding of the hard domains.

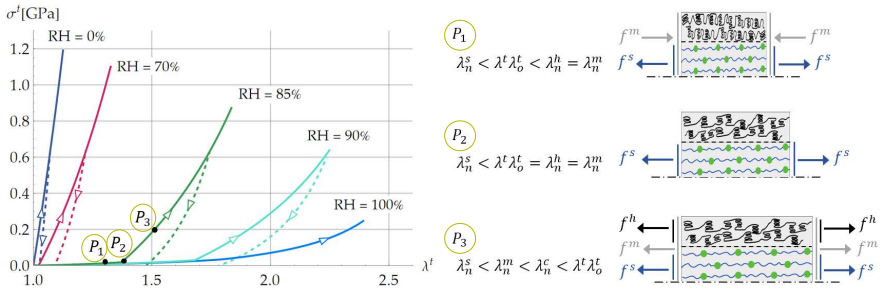


Figure 8: Theoretical stress-stretch curves at different humidity conditions (continuous lines correspond to loading and dashed to unloading curves). Three points of the curve RH = 85% are marked to illustrate different regimes schematically illustrated on the right: P_1 hard phase is unloaded, P_2 hard phase in its natural configuration, P_3 hard phase in traction. Here $E_o^h = 2.16$ GPa, $E^s = 18$ MPa, $\mu = 0.14$ MPa, $c_1 = 1.33$, $c_2 = 0.75$, $\alpha = 0.0099$, $m_f/m_o = 0.3$, $\bar{s} = 6.5$, $\lambda_c^s = 1.65, \mathrm{RH}_c = 80\%, \lambda_{lim} = 1.34$.

A comment about a second important aspect of the variable mechanical behavior is now in order: *temperature effects*. Indeed, when the temperature at fixed RH is increased, the silk undergoes an effect of link scissions as described for humidity [**?**]. Moreover, also temperature growth is accompanied by fiber contraction [**?**] and again the experiments show the existence of a critical value where such effects of link scission and length variation are strongly localized. In analogy with polymer mechanics this value is indicated as glass transition temperature T_g. In particular, in [**?**] the authors obtained an experimental linear relation between T_g and RH. Of course such a relation would ask a theoretical description that by itself appears to be very interesting, but it is out of the aims of this paper. Instead, to show that our model can reproduce also the experimental temperature effects, we *phenomenologically* assume a Gaussian dependence of the number of links from temperature in Eqn. (2) (where RH is substituted by T) and then we modify correspondingly the constitutive equation Eqn. (18). Accordingly RH_c is substituted by T_g. The efficacy of these assumptions are well supported by the experimental comparison considered in the following section.

The final aspect of the model regards the humidity and temperature depen-

dence of the limit stretch: to this hand we need a *fracture criterion*. Based on the considerations in [**?**] we here assume that the fracture is regulated by the hard fraction and in particular that the fracture condition is $\lambda^h = \lambda_{lim}$, where λ_{lim} is a given constitutive parameter. As we show in the following section, this criterion is successful with the exception of the fully dry condition where the breakage is known to be induced by localized damage defects [**?**].

3. Experimental validation

In this final section we verify the effectiveness of the proposed model in predicting the mechanical behavior of spider silks by quantitatively comparing the main experimental effects induced by humidity and temperature variations on different silks with the theoretical behavior.

Consider first the tensile response under variable RH for a highly stretchable silk (Argiope trifasciata fibers, reproduced by [**?**]). As shown in Fig. 9 this

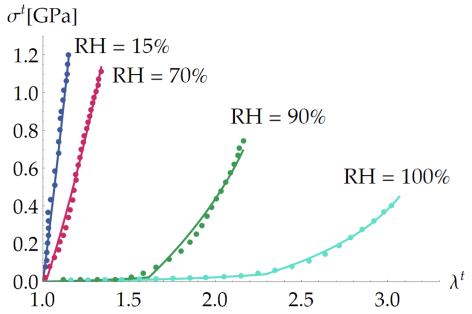


Figure 9: Theoretical (continuous lines) *vs* experimental (dots, reproduced from [**?**]) stress-stretch curves for *Argiope trifasciata* spider fibers at different RH and $T = 20\,^{\circ}$C. Here $E_o^h = 2.2$ GPa, $E^s = 13.5$ MPa, $\mu = 0.14$ MPa, $c_1 = 1.3$, $c_2 = 0.87$, $\alpha = 0.0094$, $\bar{s} = 8.5$, $m_f/m_o = 0.12$, $\lambda_c^s = 1.62$, $\lambda_{lim} = 1.34$, $\mathrm{RH}_c = 85\%$.

silk exhibits a remarkable dependence of the mechanical response on humidity. We may observe two different regimes in accordance with the silk experimental response: for RH<RH_c the behavior is almost linear and this is due in our model to the dominance of the hard fraction; for RH>RH_c we have two regimes. Initially the silk is highly stretchable, with high deformations at very low forces.

In this regime the numerical simulations show that the hard region is shorter than its natural length, so it does not contribute to the fiber stiffness. When this length is attained, the fiber exhibits a sudden hardening. In Fig. 9 it is possible also to verify the efficacy of the introduced fracture criterion. Indeed, we calibrated the hard fraction limit stretch to reproduce the experimental limit at RH = 70% and then we predicted the RH = 90% and 100% cases with errors of only 0.17% and 1.49%, respectively. As anticipated the prediction is less accurate for very low humidities. Observe the possibility of predicting damage, hardening localization and fracture strain at very different values of the humidity with fixed parameters.

To further test the efficiency of the model, we show the possibility of predicting the influence of humidity and temperature on other important material parameters, such as elastic modulus, supercontraction stretch of unrestrained fibers and limit stretches (Fig. 10). It is important to remark, regarding the predictivity properties of the model, that in this prediction of the experiments *we fixed the material parameters* and changed only RH_c at different temperatures *using the experimental values in* [**?**]. In Fig. 10 we also reproduce the limit stretch for the available testing temperature (55 ℃).

Furthermore, we consider the effects induced by variable temperature at fixed RH in [**?**]. We evaluated T_g at given RH=50% using the relation reported in the same paper. The results exhibited in Fig. 11 show again an accurate reproduction of the experiments. We remark that a comparison of the values of E at $RH = 50\%$ and different temperatures lead to different values of the elastic moduli estimated by Fig. 10 and Fig. 11, thus showing that the data refers to different silks so that different parameters have been used in the two figures.

In addition to the *Argiope trifasciata* spider fibers (Fig. 9), we consider tensile tests performed on a *Nephila clavata* spider fiber under various RHs $(0\%, 75\%, 97\%)$ reproduced from [**?**]. In Fig. 12 we report the comparison between the experimental results and the theoretical model. Despite this silk shows

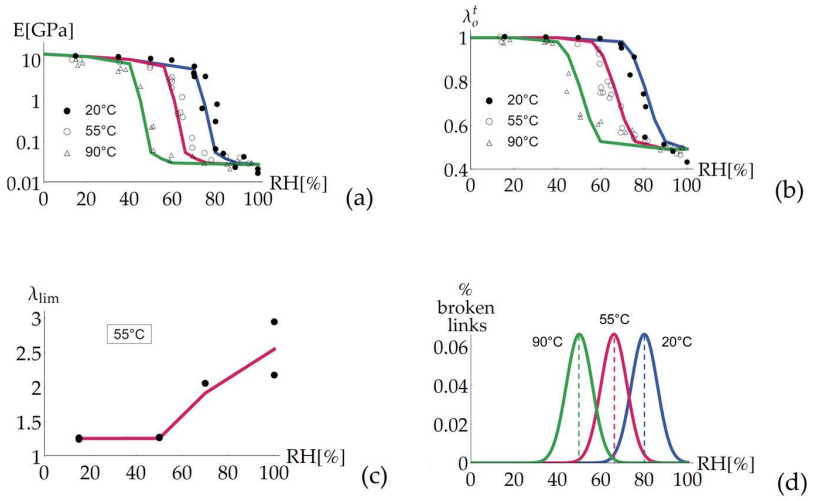


Figure 10: Theoretical (continuous lines) *vs* experimental (dots) curves for the initial elastic modulus (a), initial (zero force) stretch (b), limit stretch (c) and assumed Gaussian distribution of broken links (d) as a function of RH for *Argiope trifasciata* fibers [**?**]. Here $E_o^h = 4.05$ GPa, $E^s = 39.6$ MPa, $\mu = 0.2$ MPa, $c_1 = 1.4,\ c_2 = 0.75,\ \alpha = 0.0065,\ \bar{s} = 0.6,\ m_f/m_o = 0.23,$ $\lambda_c^s = 2.05,\ \lambda_{lim} = 1.26,$ and $\text{RH}_c = 80, 66, 50\%$ for $T = 20, 55, 90\,^{\circ}\text{C}$, respectively.

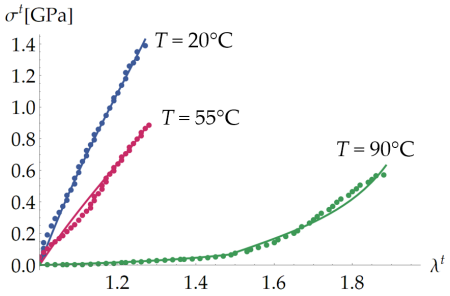


Figure 11: Theoretical (continuous lines) *vs* experimental (dots) stress-stretch curves for *Argiope trifasciata* spider fibers at different temperature at fixed RH = 50% (reproduced from [**?**]). Here $T_g = 84\,^{\circ}\text{C},\ E_o^h = 3.83$ GPa, $E^s = 32.7$ MPa, $\mu = 2$ MPa, $c_1 = 1.36,$ $c_2 = 1.25,\ \alpha = 0.00995,\ \bar{s} = 4.5,\ m_f/m_o = 0.345,\ \lambda_c^s = 1.49,\ \lambda_{lim} = 1.27.$

a remarkably different response to the humidity variations, the proposed model is once again significantly successful in quantitatively predicting the observed
255 experimental behavior. In Fig. 12 we also test the above described rupture hypothesis for the *Nephila clavata* fibers by using the value corresponding to the

experimental break at RH = 75% to predict the breaking strain at RH = 97% with an error of 0.22%. This remarkable small error confirms the plausibility of the proposed rupture criterion. Observe anyway that this hypothesis in this silk cannot be applied to the fully dry case where the breakage is typically induced by localized defects [**?**].

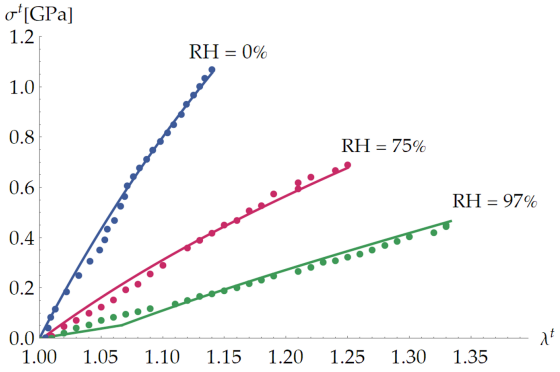


Figure 12: Theoretical (continuous lines) *vs* experimental (dots) stress-stretch curves for *Nephila clavata* fibers at different humidity and $T = 25\,^{\circ}$C (reproduced from the experiments at strain rate of $3.3 \times 10^{-3}\ s^{-1}$ in [**?**]). Here $E_o^h = 5.6$ GPa, $E^s = 1.47$ GPa, $\mu = 1.1$ MPa, $c_1 = 1.35,\ c_2 = 1.46,\ \alpha = 0.009, m_f/m_o = 0.878,\ \bar{s} = 3,\ \lambda_c^s = 4.6, \lambda_{lim} = 1.25,\ \mathrm{RH}_c = 80\%$.

As a last comparison with experimental results, in Fig. 13 we show the possibility of predicting with remarkable accuracy the complex mechanical response of a dragline silk in dry condition (reproduced from [**?**]). Notice that here, the thread is produced by a third species of spider, the *Araneus diadematus*.

4. Discussion

A comment is in order. As anticipated previously, in the recent paper [**?**] the authors proposed a different model well reproducing with 8 parameters the experiments in Fig.10a),b). Our model, being based on a more detailed description of the microstructure, considering the two different fractions and stretch induced unfolding effects, ends up with 10 parameters. On the other hand, the proposed model is able to reproduce the whole stress-strain curves as function of both temperature and humidity, with unloading, increasing damage,

fracture and residual stretches. It's important to observe that the most diffuse models efficiently describing damage and residual stretches in soft polymeric materials (without any temperature and humidity effects) adopt 7-8 parameters (see [**?**] and references therein).

5. Conclusions

The described ability of the proposed model of predicting the experimental behavior of different mechanical properties make us confident that it well reproduces the humidity and temperature effects at the molecular scales. This is supported even more by predicting the behavior of different silks and environmental conditions. We strongly believe that this is a consequence of our microstructure deduction of the material response function. The physical meaning of all the adopted (microscopic) parameters opens up the possibility of applying the proposed model not only to other protein materials with similar structures [**?**], but also in the design of bioinspired materials employing chosen specific proteins [**? ?**].

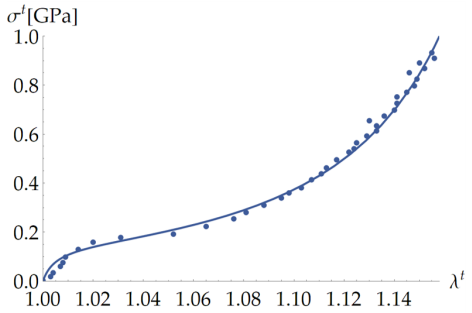


Figure 13: Theoretical (continuous lines) *vs* experimental (dots) stress-stretch curves for *Araneus diadematus* spider fibers (reproduced from [**?**]). Here $E_o^h = 6.75$ GPa, $E^s = 13.6$ MPa, $\mu = 1$ MPa, $c_1 = 1.005$, $c_2 = 1.979$, $\alpha = 0$, $m_f/m_o = 0.13$, $\bar{s} = 4.5$, $\lambda_c^s = 1.25$, $\mathrm{RH}_c = 84\%$.

Declaration of Competing Interest

The authors declare that they have no known competing financial interests or personal relationships that could have appeared to influence the work reported in this paper.

Acknowledgments

The authors thank G. Greco for insightful discussions on the subject of the paper and for indicating important papers missing in the previous version including the very recent article [**?**]. Funding: GP has been supported by the Italian Ministry MIUR-PRIN project 2017KL4EF3 and by GNFM (INdAM), DD by the Italian Ministry MIUR-PRIN project 2017J4EAYB and NMP by the European Commission under the FET Open "Boheme" grant no. 863179 and by the Italian Ministry of Education MIUR under the PON ARS01-01384-PROSCAN Grant and the PRIN-20177TTP3S.